

Article

Submicron Sized Nb Doped Lithium Garnet for High Ionic Conductivity Solid Electrolyte and Performance of All Solid-State Lithium Battery

Yan Ji ¹, Cankai Zhou ¹, Feng Lin ¹, Bingjing Li ¹, Feifan Yang ¹, Huali Zhu ², Junfei Duan ¹ and Zhaoyong Chen ^{1,*}

¹ College of Materials Science and Engineering, Changsha University of Science and Technology, Changsha 410114, China; juefly@stu.csust.edu.cn (Y.J.); zhoucankai@stu.csust.edu.cn (C.Z.); 18216359528@163.com (F.L.); krystalbingjingli@163.com (B.L.); yff_0413@126.com (F.Y.); junfei_duan@csust.edu.cn (J.D.)

² College of Physics and Electronic Science, Changsha University of Science and Technology, Changsha 410114, China; juliezhu2005@126.com

* Correspondence: chenzhaoyongcioc@126.com

Abstract: The garnet $\text{Li}_7\text{La}_3\text{Zr}_2\text{O}_{12}$ (LLZO) has been widely investigated because of its high conductivity, wide electrochemical window and chemical stability to lithium metal. However, the usual preparation process of LLZO requires a long time of high-temperature sintering and a lot of mother powders against the lithium evaporation. The submicron $\text{Li}_{6.6}\text{La}_3\text{Zr}_{1.6}\text{Nb}_{0.4}\text{O}_{12}$ (LLZNO) powders are prepared by conventional solid-state reaction method and attrition milling process, which are stable cubic phase and have high sintering activity, and Li stoichiometric LLZNO ceramics are obtained by sintering at a relative lower temperature or for a short time by using these powders which are difficult to control under high sintering temperature and long sintering time. The particle size distribution, phase structure, microstructure, distribution of element, total ionic conductivity, relative density and activation energy of submicron LLZNO powders and LLZNO ceramics are tested and analyzed by laser diffraction particle size analyzer, XRD, SEM, EIS and Archimedean method. The total ionic conductivity of sample sintered at 1200 °C for 30 min is $5.09 \times 10^{-4} \text{ S}\cdot\text{cm}^{-1}$, the activation energy is 0.311 eV, and the relative density is 87.3%, and sintered at 1150 °C for 60 min total ionic conductivity is $3.49 \times 10^{-4} \text{ S}\cdot\text{cm}^{-1}$, the activation energy is 0.316 eV, and the relative density is 90.4%. At the same time, all-solid-state batteries are assembled with LiMn_2O_4 as positive electrode and submicron LLZNO powders as solid state electrolyte. After 50 cycles, the discharge specific capacity is 105.5 mAh/g and the columbic efficiency is above 95%.

Keywords: Solid State Electrolyte; Submicron Powders; Garnet; Lithium Ion Conductivity; Solid-State Batteries

1. Introduction

Currently, lithium-ion batteries are widely used in EVs, HEVs, computers, smart grids, wearable devices, and so on. The traditional lithium ion batteries with organic liquid electrolyte easily burnt and exploded under abuse conditions. In addition, with the development of modern society, lithium-ion batteries are gradually toward to high specific energy. Researchers studied cathode materials to increase the energy density of lithium-ion batteries, such as $\text{LiNi}_{0.33}\text{Co}_{0.33}\text{Mn}_{0.33}\text{O}_2$, $\text{LiNi}_{0.5}\text{Co}_{0.2}\text{Mn}_{0.3}\text{O}_2$, $\text{LiNi}_{0.6}\text{Co}_{0.2}\text{Mn}_{0.2}\text{O}_2$, $\text{LiNi}_{0.8}\text{Co}_{0.1}\text{Mn}_{0.1}\text{O}_2$, $\text{LiNi}_{0.8}\text{Co}_{0.15}\text{Al}_{0.05}\text{O}_2$, $x\text{Li}_2\text{MnO}_3\cdot(1-x)\text{LiMO}_2$, [1-7] etc. The energy density can be improved by improving the charging voltage, which will lead to serious side reactions and safety issues. In order to solve the safety problem of lithium-ion batteries, the researchers paid their attention to all-solid-state lithium batteries with inorganic electrolyte; The nonignition, long cycling life and wide electrochemical window of all-solid-state lithium batteries are considered to satisfy the high safety and high energy density of the next-generation energy storage systems.

Solid electrolyte is an important component of all-solid-state batteries, which can not only be used as lithium ionic conductor in the charge-discharge process of batteries, but also can be used as separator to block the direct contact between positive and negative electrodes. Solid electrolytes generally have Li_3N , LiPON , perovskite, LISICON, NASICON, garnet, etc. [8-13] Some of these solid electrolytes have high ionic conductivity ($\sim 10^{-3} \text{ S}\cdot\text{cm}^{-1}$), however, there are some issues still existing, such as the instability of ambient atmosphere (LGPS), metal cation is easily to be reduced by metal lithium (LLTO), etc.[14] The cubic garnet LLZO is discovered by Murugan et al[13] in 2007, which attracted world-wide attention for its advantages. For example, simple preparation process, high ionic conductivity ($\sim 10^{-3} \text{ S}\cdot\text{cm}^{-1}$) at room temperature, high electrochemical window (0~ 6 V vs. Li/Li^+), electrochemical stability of lithium metal and so on. On the other hand, LLZO also has some defects, such as unstable cubic phase and low density of ceramics[15,16]. Moreover, a mass of LLZO mother powders are needed to compensate lithium loss when sintering at high-temperature[16,17]. Many solutions had adopted to solve above issues. For example, doping Al, Ga, Fe, Ta, Nb, W, Y, Sb to stabilize the cubic phase;[18-25] Adopting hot pressing sintering, plasma sintering and microwave sintering to increase the relative density and sintering additives[26-28]; Investigating Y_2O_3 , Al_2O_3 , B_2O_3 , CaO, MgO, Li_3PO_4 and Li_4SiO_4 to reduce the grain boundary resistance[29-35].

In this paper, the submicron LLZNO powders with stable cubic phase is synthesized by the conventional solid-state reaction method and prepared by the following attrition milling process. The submicron LLZNO powders have a higher sintering activity, which can promote the sintering process, reduce sintering temperature and time and reduce the loss of Li at high-temperature sintering, all these characteristics are in favor of the lithium stoichiometry and ionic conductivity. What's more, the LLZNO ceramics without the mother powders are obtained when sintering temperature and time are reduced. The particles size distribution, phase structure, microtopography, total ionic conductivity, relative density and activation energy are characterized and analyzed. The all-solid-state lithium batteries with LiMn_2O_4 as positive electrode and submicron LLZNO powders as solid electrolyte are assembled and the electrochemical performances are also tested and analyzed.

2. Materials and Methods

1.1 The synthesis of LLZNO powders and ceramics

Process flow chart of preparation of submicron LLZNO powders and sintering of LLZNO ceramics is showed in Figure 1. LLZNO powders are synthesized by traditional solid phase method[36]. Lithium hydroxide monohydrate ($\text{LiOH}\cdot\text{H}_2\text{O}$, 98%, Xilong Scientific Co., Ltd.), Lanthanum oxide (La_2O_3 , 99.99%, Aladdin), zirconia (ZrO_2 , 99%, Aladdin), Niobium oxide (Nb_2O_5 , 99.99%, Sinopharm Chemical Reagent Co., Ltd.) is used as the raw material and 10wt% excess of $\text{LiOH}\cdot\text{H}_2\text{O}$ is added to compensate the lithium loss in high-temperature calcination and sintering process. Yttrium stabilized zirconia (YSZ, 4~ 8 mm in diameter) and isopropanol (IPA) are used as the ball grinding medium. The ratio of raw material and grinding balls is 1:5 and the mixed raw material powders are wet-ball grinded at 800 rpm in the planetary ball mill for 6 h. The mixture is dried at 70 °C for 14 h, then calcined at 950 °C for 12 h in an alumina crucible with ambient air to obtain the cubic phase LLZNO powders. LLZNO slurry is attrition milled (Shanghai ROOT mechanical and electrical equipment Co., Ltd., 0.7l volume, 70% filling rate) at 1000 rpm for 2 h, taking YSZ (0.4 mm in diameter) and IPA as grinding medium and a solid-liquid ratio is 1:5. The submicron LLZNO slurry is dried at 70 °C for 14 h and green pellets (mass of 3 g, 19 mm in diameter and thickness of about 4 mm) are pressed at 200 Mpa under the cold uniaxial press. After that, the green pellets without mother powders are sintered in muffle furnace (Changsha Yuandong Electric Furnace Factory) at 1100- 1200 °C for 30- 360 min, and then cool down naturally. At the same time, the green pellets are putted upon the platinum wire and placed in the crucible of MgO with the lid to prevent impurity migration and a large amount of volatilization of lithium in the process of high-temperature sintering. For further testing, LLZNO ceramics pellets are polished with 400 and 1000 mesh sandpaper.

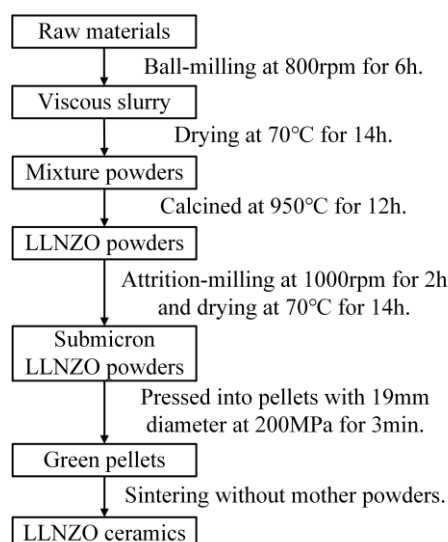


Figure 1. Process flow chart for preparation of submicron LLZNO powders and sintering of LLZNO ceramics.

1.2 Fabrication of composite electrode and assembly of all-solid-state batteries

The composite electrode consists of the LiMn_2O_4 positive electrode layer and the submicron LLZNO electrolyte layer. The positive electrode is fabricated by coating the slurry of a mixture containing LiMn_2O_4 powders, submicron LLZNO powders, acetylene black and polyvinylidene difluoride (PVDF) with a weight ratio of 7:2:1:1 onto circular aluminum foils as current collector. Then the composite electrode is fabricated by coating the slurry of a mixture containing submicron LLZNO powders and PVDF with a weight ratio of 9:1 onto positive electrode layer. And composite electrode is punched into disks with 18 mm diameter after compacted by a roller press. All-solid-state batteries are assembled in the glove box full of argon fulfill, and metal lithium foil (15 mm in diameter and thickness of 1 mm) as negative current collector. In addition, composite electrode is wetted with 20 μL organic electrolyte to reduce the interface impedance.

1.3 Characterization

X-ray diffraction (XRD, Cu-K α radiation, $\lambda=1.542 \text{ \AA}$, Bruker D8 ADVANCE) is used to determine the phase of ceramics pellets at room temperature within 10- 60 $^\circ$ with the step of 5 $^\circ$ /min. Jade software is used to match and analyze the phase of the sample. The relative density of ceramics is measured by Archimedes method and deionized water is used as the immersion medium. Meanwhile, the theoretical density of LLZNO is 5.20 g/cm^3 which calculated by jade software, and the relative density is measured density divided by the theoretical density. The particle size and distribution of the powders are determined by the laser particle size test method (LD, Mastersizer 3000) and the relative density, refractive index and absorption rate of LLZNO powders is 5.20 g/cm^3 , 1.4 and 0.1, respectively. The microtopography of submicron LLZNO powders and cross-section of the ceramic pellets are observed by scanning electron microscope (SEM, TESCAN MIRA3 LMU). Energy dispersive spectrometer (EDS, Oxford X-ray Max20) mapping is used to characterize the distribution of each element in the cross-section of ceramic pellets. The total lithium ion conductivity of ceramic pellets is measured by AC impedance method (EIS, Gamry Reference 600+) at the temperature range of 25- 80 $^\circ\text{C}$ within the frequency of 10 Hz-5 MHz of and with AC amplitude of 40 mV. The blocking electrode is uniformly coated by thin silver layer on both sides of ceramic pellets. The activation energy of ceramic pellets is measured at the temperature range of 25- 80 $^\circ\text{C}$ and calculated based on the Arrhenius equation. The all-solid-state batteries are tested under the batteries charge-discharge tester (BTS-5V3A, Neware Technology Co., Ltd.) at 25 $^\circ\text{C}$ and current density is 0.02 mA/cm^2 .

3. Results and Discussions

XRD pattern of LLZNO powders is showed in Figure 2c and identified as cubic phase (PDF 63-0174). The LD result and SEM image of LLZNO powders after attrition milling process which are demonstrated as submicron powders and showed in Figure 2a, Table.1 and Figure 2b. The $D_{(10)}$, $D_{(50)}$, $D_{(90)}$ and primary particle's size of submicron LLZNO powders are $0.43\ \mu\text{m}$, $0.59\ \mu\text{m}$, $0.812\ \mu\text{m}$ and about $0.1\ \mu\text{m}$, respectively. The value of $D_{(3,2)}$ ($0.575\ \mu\text{m}$) is similar to $D_{(4,3)}$ ($0.607\ \mu\text{m}$), which indicates that the prepared powders has a uniform particle size distribution. In addition, the powders also have a higher specific surface area ($2007\ \text{m}^2/\text{kg}$), it means that the powders have a higher sintering activity, which can promote the crystal growth and the rapid densification of ceramics in the sintering process.

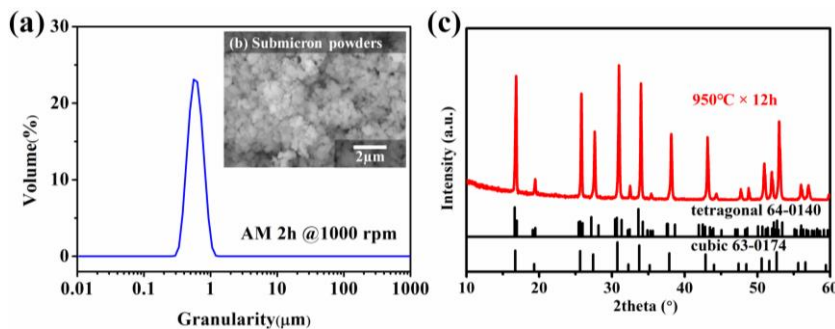


Figure 2. (a) Particle sizes distribution of LLZNO powders after attrition milled 2h at 1000rpm and (b) SEM images; (c) XRD pattern of LLZNO powders.

Table 1. Laser particle size test results of submicron-scale LLZNO powders.

Preparation condition	D_{10} (μm)	D_{50} (μm)	D_{90} (μm)	$D_{[3,2]}$ (μm)	$D_{[4,3]}$ (μm)	Specific surface area (m^2/kg)
Attrition milled 2h @ 1000 rpm	0.430	0.590	0.812	0.575	0.607	2007

The XRD patterns of LLZNO ceramic samples are showed in Figure 3. The phases of all the prepared ceramic samples are identified as cubic phase (PDF 63-0174). The crystal parameters of different samples are showed in Table 1. The XRD patterns of $1200\ \text{C} \times 60\ \text{min}$ and $1100\ \text{C} \times 360\ \text{min}$ shows a little impure phase peaks, which mainly belongs to LiNbO_3 (PDF 82-0459) and Li_7NbO_6 (PDF 29-0816) due to the decomposition of high sintering activity LLZNO after sintered for too long time at a higher temperature.

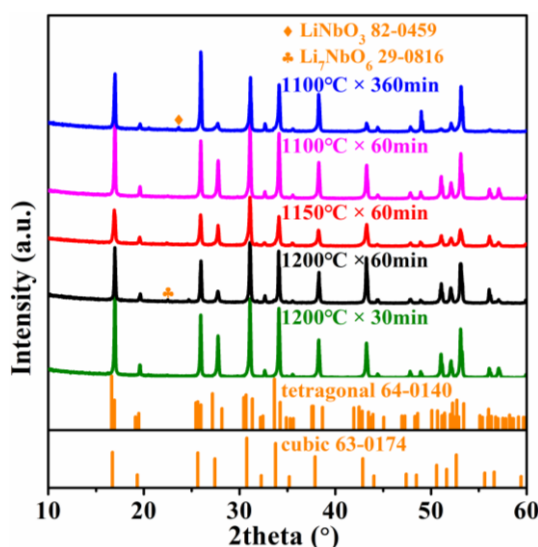


Figure 3. XRD patterns of the LLZNO ceramics with different sintering conditions.

AC impedance plots and its enlargement of LLZNO ceramic pellets at different sintering conditions are showed in Figure 4a and Figure 4b. Equivalent circuit model $R_b(R_{gb}Q_{gb})(R_{el}Q_{el})$ is used to fit the plots and showed in the Figure 4d, in which R_b , R_{gb} , and R_{el} are resistances originated from bulk, grain boundaries and Ag electrodes; The fitting curve of $1200\text{ }^\circ\text{C} \times 30\text{ min}$ is showed in Figure 4c, and it consists of a quasi-semicircle at high frequency and a long diffusion tail at low frequency. The total ionic conductivity of ceramics is mainly decided by R_b plus R_{gb} . The total ionic conductivity and relative density of LLZNO ceramic pellets are showed in Figure 4e and Table 1. The highest total ionic conductivity ($5.09 \times 10^{-4}\text{ S}\cdot\text{cm}^{-1}$) of LLZNO ceramic pellets is obtained when sintered at a higher temperature and in a shorter time ($1200\text{ }^\circ\text{C} \times 30\text{ min}$), and its relative density is 87.3%. However, the total ionic conductivity and relative density of ceramic pellets are decreased when prolonging the sintering time at $1100\text{ }^\circ\text{C}$ and $1200\text{ }^\circ\text{C}$, and the lowest total ionic conductivity ($0.35 \times 10^{-4}\text{ S}\cdot\text{cm}^{-1}$) and relative density (83.4%) are obtained when sintered at $1100\text{ }^\circ\text{C}$ for 360 min. Meanwhile, a higher total ionic conductivity ($3.49 \times 10^{-4}\text{ S}\cdot\text{cm}^{-1}$) and a higher relative density (90.3%) of ceramic pellets ($1150\text{ }^\circ\text{C} \times 60\text{ min}$) are obtained when sintered for 60 min at sintering temperature from $1100\text{ }^\circ\text{C}$ to $1200\text{ }^\circ\text{C}$, which indicates that it is disadvantaged to increase the sintering temperature too much in this paper.

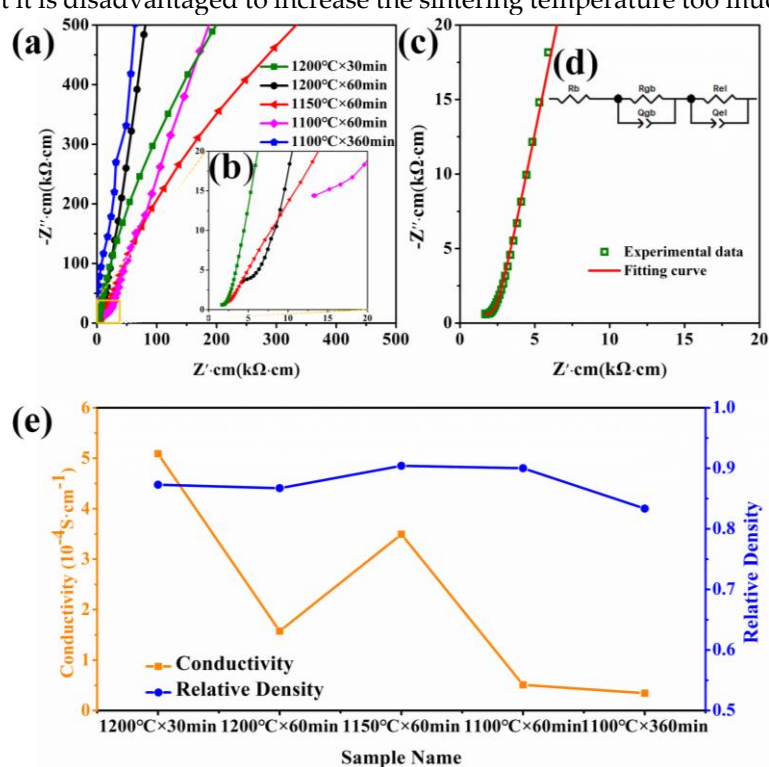


Figure 4. (a-b) AC impedance plots of the LLZNO ceramics with different sintering conditions at $25\text{ }^\circ\text{C}$; (c) AC impedance plots and fitting curve of $1200\text{ }^\circ\text{C} \times 30\text{ min}$ at $25\text{ }^\circ\text{C}$; (d) Equivalent circuit to fit the curves. (e) Conductivity and relative density of the LLZNO ceramics.

Table 2. Sintering condition, cell parameter, total ionic conductivity at $25\text{ }^\circ\text{C}$, activation energy and relative density of LLZNO ceramics.

Sintering condition	Cell parameter (Å)	Total ionic conductivity ($10^{-4}\text{ S}\cdot\text{cm}^{-1}$), $25\text{ }^\circ\text{C}$	Activation energy (eV)	Relative density
$1200\text{ }^\circ\text{C} \times 30\text{ min}$	12.8953	5.09	0.311	87.3%
$1200\text{ }^\circ\text{C} \times 60\text{ min}$	12.8952	1.58	0.315	86.7%
$1150\text{ }^\circ\text{C} \times 60\text{ min}$	12.9028	3.49	0.316	90.4%
$1100\text{ }^\circ\text{C} \times 60\text{ min}$	12.8916	0.51	0.319	90.3%
$1100\text{ }^\circ\text{C} \times 360\text{ min}$	12.8870	0.35	0.328	83.4%

Arrhenius plots and its linear fitting curves are showed in Figure 5a. The activation energy of ceramics samples is showed in Figure 5b and Table 1, and their values are within the range of 0.31–0.33 eV. This indicates that there is no obvious affection to activation energy of ceramics when the green pellets prepared by submicron LLZNO powders are sintered. The variation tendency of activation energy is similarity to total ionic conductivity, and the lowest and the highest activation energy is 0.311 eV ($1200\text{ }^{\circ}\text{C} \times 30\text{ min}$) and 0.328 eV ($1100\text{ }^{\circ}\text{C} \times 360\text{ min}$).

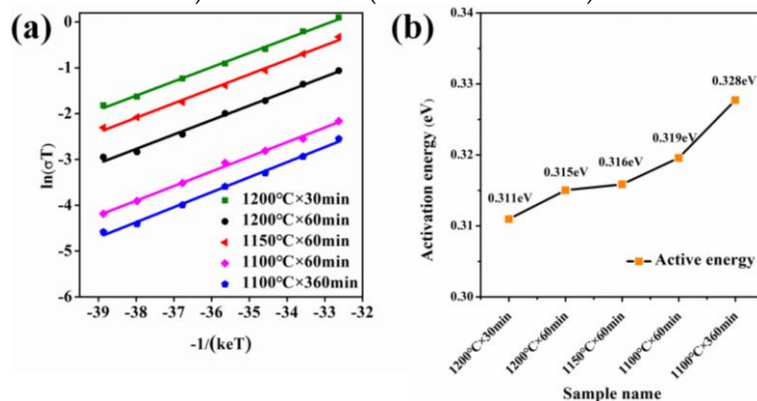


Figure 5. (a) Arrhenius plots and fitting results; (b) Activation energy of different LLZNO ceramics.

SEM images of LLZNO ceramics cross-section which sintered at different sintering conditions are showed in Figure 6a–6e. We can find that the grain size of ceramics which sintered for 60 min at temperature range of $1100\text{ }^{\circ}\text{C}$ to $1200\text{ }^{\circ}\text{C}$ gradually grows from $1\text{--}5\text{ }\mu\text{m}$ ($1100\text{ }^{\circ}\text{C} \times 60\text{ min}$, Figure 6a) to a little of grains are $5\text{ }\mu\text{m}$ and most of grains are $100\text{--}200\text{ }\mu\text{m}$ ($1150\text{ }^{\circ}\text{C} \times 60\text{ min}$, Figure 6c), and finally, all grains are about $200\text{ }\mu\text{m}$ ($1200\text{ }^{\circ}\text{C} \times 60\text{ min}$, Figure 6d). Here, we find a mass of abnormal growth grains (AGG) in Figure 6b–6d and a mass of pores are distributed in AGG, and meanwhile, the total ionic conductivity is lower when AGG is bigger. That is due to the submicron LLZNO powders have a higher sintering activity, which makes the crystal grain of LLZNO ceramics have high specific surface energy during high-temperature sintering process, and promotes the grains grow and ceramics densification rapidly in the sintering process. For the above reasons, the growth rate of grains is higher than the migration rate of pores at grain boundaries when sintering temperature is higher and sintering time is longer, and the pores cannot be discharged from the grain boundaries and finally stay in the inside of AGG. As a result, the bulk impedance of the crystal grains is increased, and the total ion conductivity is reduced. However, although the submicron LLZNO powders have high sintering activity, the growth of grains cannot be entirely promoted in a shorter sintering time and at a lower temperature. So a mass of grains which stay at initial state are showed in Figure 6a ($1100\text{ }^{\circ}\text{C} \times 60\text{ min}$), and that is disadvantageous for lithium ionic conduction due to incomplete surface of LLZNO grains after attrition milling process. Eventually, the ceramic pellets show a lower total ionic conductivity ($0.51 \times 10^{-4}\text{ S}\cdot\text{cm}^{-1}$). A cross-section SEM image of $1200\text{ }^{\circ}\text{C} \times 30\text{ min}$ is showed in Figure 6e, it can be found that the grains grow uniformly ($\sim 4\text{ }\mu\text{m}$), surface is smooth without pores and bond tightly with other grains. And the highest ionic conductivity of $5.09 \times 10^{-4}\text{ S}\cdot\text{cm}^{-1}$ is obtained, and which indicates that the submicron LLZNO powders have a higher sintering activity, and high total ionic conductivity LLZNO ceramic pellets can be obtained by sintered at a high temperature only for a short time. At the same time, the LLZNO ceramic pellets which have a higher total ionic conductivity also can be also obtained when reduce the sintering temperature properly.

Figure 6f shows the SEM image and its EDS mapping including La, Zr, and Nb in cross-section of LLZNO ceramic of $1200\text{ }^{\circ}\text{C} \times 30\text{ min}$. The cross-section of the sample exhibits transgranular fracture and intergranular fracture, and the elements of La, Zr, and Nb are uniformly distributed, which indicates that the Nb element is successfully incorporated into the LLZO lattice, and that is also verified by the XRD result without impure phase.

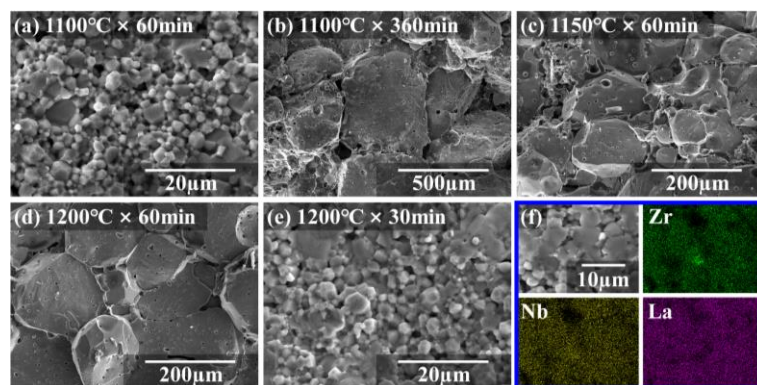


Figure 6. (a-e) SEM images of cross-sectional microstructure of ceramics which sintering by different particles sizes at different sintering conditions; (f) EDS mapping of LLZNO ceramics section sintered at 1200 °C for 30 minutes.

Specific capacity and coulombic efficiency of all-solid-state batteries with LiMn_2O_4 as the positive electrode after 50 cycles galvanostatic charge-discharge test at 25 °C are showed in Figure 7a. And the 1st, 2nd, 10th, 20th, and 50th galvanostatic charge-discharge curves of all-solid-state batteries are showed in Figure 7b. The all-solid-state batteries show good cycling performance at current density of 0.02 mA/cm² and voltage within 3.0- 4.3 V. The 1st discharge specific capacity is 106.4 mAh/g, and coulomb efficiency is 93.23%. And the 2nd, 10th, 20th, and 50th discharge specific capacity is 106.8 mAh/g, 105.3 mAh/g, 106.9 mAh/g and 105.5 mAh/g, respectively. After 50 cycles galvanostatic charge-discharge test, the coulomb efficiency is maintained at about 95%, the capacity retention rate is 99.15%. The capacity of the batteries increased in the early stage of the galvanostatic charge-discharge test, which may be caused by the activation of positive material. This indicates that sub-micron LLZNO powders can be used in all-solid-state batteries, and the specific capacity and the cycling stability of all-solid-state batteries are relatively good.

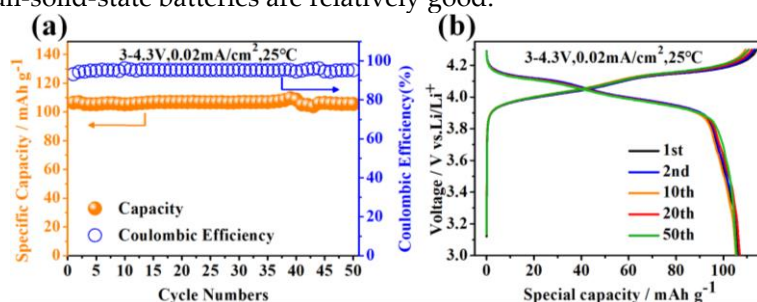


Figure 7. (a) Specific capacity and coulombic efficiency; (b) The 1st, 2nd, 10th, 20th, and 50th galvanostatic charge-discharge curves of all-solid-state batteries with LiMn_2O_4 as the positive electrode.

4. Conclusions

In this paper, we synthesized Nb-doped stabilized cubic phase LLZO powders by the conventional solid-state reaction method, and prepared submicron LLZNO powders by the attrition milling process. Electrolyte ceramics prepared by submicron LLZNO powders can be sintered without mother powders, reduce the sintering temperature and shorten the sintering time. After sintered at 1150 °C for 60 min, the total ionic conductivity, relative density and activation energy is $3.49 \times 10^{-4} \text{ S}\cdot\text{cm}^{-1}$, 90.4%, and 0.316 eV, respectively. When sintered at 1200 °C for 30 min, we obtained the highest total ionic conductivity is $5.09 \times 10^{-4} \text{ S}\cdot\text{cm}^{-1}$, and the relative density is 87.3%, and the smallest activation energy is 0.311 eV. For the all-solid-state batteries prepared with submicron LLZNO powders, the capacity retention rate is 99.15% and specific capacity is 105.5 mAh/g after 50 cycles at room temperature with current density of 0.02 mA/cm². Therefore, we have a simple method to reduce the rate of raw materials and energy when sintering LLZO ceramics. At the same time, the prepared submicron LLZO powders can be also used in the preparation of all-solid-state batteries.

Author Contributions: Methodology and Conceptualization, Z.C., Y.J., and C.Z.; Resources, Z.C. and H.Z.; Data Curation, Y.J., C.Z., F.L., B.L., and F.Y.; Writing—Original Draft Preparation, Y.J.; Writing—Review and Editing, Y.J. and J.D.; Funding Acquisition, Z.C. and H.Z.

Funding: This work was supported by the National Natural Science Foundation of China (No. 51874048), the National Science Foundation for Young Scientists of China (No. 51604042), the Research Foundation of Education Bureau of Hunan Province (No.19A003) and Scientific Research Fund of Changsha Science and Technology Bureau (No. kq1901100) and Postgraduate Innovative Test Program of Hunan Province.

Conflicts of Interest: The authors declare no conflict of interest.

References

1. Zhu, H.; Jie, L. I.; Chen, Z.; Qifeng, L. I.; Tian, X.; Lingjun, L. I.; Lai, Y. Molten salt synthesis and electrochemical properties of LiNi_{1/3}Co_{1/3}Mn_{1/3}O₂ cathode materials. *Synthetic Metals* **2014**, *187*, 123-129.
2. Chen, Z.; Gong, X.; Zhu, H.; Cao, K.; Liu, Q.; Liu, J.; Li, L.; Duan, J. High performance and structural stability of K and Cl co-doped LiNi_{0.5}Co_{0.2}Mn_{0.3}O₂ cathode materials in 4.6 voltage. *Frontiers in chemistry* **2018**, *6*,
3. Chen, Y.; Zhang, Y.; Chen, B.; Wang, Z.; Lu, C. An approach to application for LiNi_{0.6}Co_{0.2}Mn_{0.2}O₂ cathode material at high cutoff voltage by TiO₂ coating. *Journal of Power Sources* **2014**, *256*, 20-27.
4. Xiong, X.; Wang, Z.; Yue, P.; Guo, H.; Wu, F.; Wang, J.; Li, X. Washing effects on electrochemical performance and storage characteristics of LiNi_{0.8}Co_{0.1}Mn_{0.1}O₂ as cathode material for lithium-ion batteries. *Journal of Power Sources* **2013**, *222*, 318-325.
5. Chen, Z.; Cao, K.; Zhu, H.; Duan, J.; Li, L.; Gong, X.; Liu, Q. Improved electrochemical performance of surface coated LiNi_{0.8}Co_{0.15}Al_{0.05}O₂ with polypyrrole. *Frontiers in chemistry* **2018**, *6*, 648.
6. Chen, Z.; Yan, X.; Xu, M.; Cao, K.; Zhu, H.; Li, L.; Duan, J. Building honeycomb-like hollow microsphere architecture in a bubble template reaction for high-performance lithium-rich layered oxide cathode materials. *ACS applied materials & interfaces* **2017**, *9*, 30617-30625.
7. Liu, J.; Liu, Q.; Zhu, H.; Lin, F.; Ji, Y.; Li, B.; Duan, J.; Li, L.; Chen, Z. Effect of Different Composition on Voltage Attenuation of Li-Rich Cathode Material for Lithium-ion Batteries. **2019**,
8. Alpen, U. v.; Rabenau, A.; Talat, G. Ionic conductivity in Li₃N single crystals. *Applied Physics Letters* **1977**, *30*, 621-623.
9. Senevirathne, K.; Day, C. S.; Gross, M. D.; Lachgar, A.; Holzwarth, N. A new crystalline LiPON electrolyte: Synthesis, properties, and electronic structure. *Solid State Ionics* **2013**, *233*, 95-101.
10. Uhlmann, C.; Braun, P.; Illig, J.; Weber, A.; Ivers-Tiffée, E. Interface and grain boundary resistance of a lithium lanthanum titanate (Li_{3-x}La_{2/3-x}TiO₃, LLTO) solid electrolyte. *Journal of Power Sources* **2016**, *307*, 578-586.
11. Kanno, R.; Murayama, M. Lithium Ionic Conductor Thio-LISICON: The Li₂S-GeS₂-P₂S₅ System. *Journal of the electrochemical society* **2001**, *148*, A742-A746.
12. Lai, Y.; Sun, Z.; Jiang, L.; Hao, X.; Jia, M.; Wang, L.; Liu, F. Rapid sintering of ceramic solid electrolytes LiZr₂(PO₄)₃ and Li_{1.2}Ca_{0.1}Zr_{1.9}(PO₄)₃ using a microwave sintering process at low temperatures. *Ceramics International* **2019**, *45*, 11068-11072.
13. Murugan, R.; Thangadurai, V.; Weppner, W. Fast lithium ion conduction in garnet-type Li₇La₃Zr₂O₁₂. *Angewandte Chemie International Edition* **2007**, *46*, 7778-7781.
14. Famprikis, T.; Canepa, P.; Dawson, J. A.; Islam, M. S.; Masquelier, C. Fundamentals of inorganic solid-state electrolytes for batteries. *Nature materials* **2019**, 1-14.
15. Awaka, J.; Kijima, N.; Kataoka, K.; Hayakawa, H.; Ohshima, K.-i.; Akimoto, J. Neutron powder diffraction study of tetragonal Li₇La₃Hf₂O₁₂ with the garnet-related type structure. *Journal of Solid State Chemistry* **2010**, *183*, 180-185.

16. Huang, Z.; Liu, K.; Chen, L.; Lu, Y.; Li, Y.; Wang, C. A. Sintering behavior of garnet-type $\text{Li}_6\text{.4La}_3\text{Zr}_1\text{.4Ta}_0\text{.6O}_{12}$ in Li_2CO_3 atmosphere and its electrochemical property. *International Journal of Applied Ceramic Technology* **2017**, *14*, 921-927.
17. Ren, Y.; Deng, H.; Chen, R.; Shen, Y.; Lin, Y.; Nan, C.-W. Effects of Li source on microstructure and ionic conductivity of Al-contained $\text{Li}_6\text{.75La}_3\text{Zr}_1\text{.75Ta}_0\text{.25O}_{12}$ ceramics. *Journal of the European Ceramic Society* **2015**, *35*, 561-572.
18. Tsai, C.-L.; Dashjav, E.; Hammer, E.-M.; Finsterbusch, M.; Tietz, F.; Uhlenbruck, S.; Buchkremer, H. P. High conductivity of mixed phase Al-substituted $\text{Li}_7\text{La}_3\text{Zr}_2\text{O}_{12}$. *Journal of electroceramics* **2015**, *35*, 25-32.
19. Janani, N.; Deviannapoorani, C.; Dhivya, L.; Murugan, R. Influence of sintering additives on densification and Li^+ conductivity of Al doped $\text{Li}_7\text{La}_3\text{Zr}_2\text{O}_{12}$ lithium garnet. *Rsc Advances* **2014**, *4*, 51228-51238.
20. Jin, Y.; McGinn, P. J. Al-doped $\text{Li}_7\text{La}_3\text{Zr}_2\text{O}_{12}$ synthesized by a polymerized complex method. *Journal of Power Sources* **2011**, *196*, 8683-8687.
21. Huang, M.; Shoji, M.; Shen, Y.; Nan, C.-W.; Munakata, H.; Kanamura, K. Preparation and electrochemical properties of Zr-site substituted $\text{Li}_7\text{La}_3(\text{Zr}_2-x\text{M}_x)\text{O}_{12}$ ($\text{M} = \text{Ta}, \text{Nb}$) solid electrolytes. *Journal of Power Sources* **2014**, *261*, 206-211.
22. Ohta, S.; Kobayashi, T.; Asaoka, T. High lithium ionic conductivity in the garnet-type oxide $\text{Li}_{7-x}\text{La}_3(\text{Zr}_2-x, \text{Nb}_x)\text{O}_{12}$ ($x = 0-2$). *Journal of Power Sources* **2011**, *196*, 3342-3345.
23. Cao, Z.-Z.; Ren, W.; Liu, J.-R.; LI, G.-R.; GAO, Y.-F.; FANG, M.-H.; HE, W.-Y. Microstructure and ionic conductivity of Sb-doped $\text{Li}_7\text{La}_3\text{Zr}_2\text{O}_{12}$ ceramics. *J Inorg Mater* **2014**, *29*, 220-224.
24. Deviannapoorani, C.; Shankar, L. S.; Ramakumar, S.; Murugan, R. Investigation on lithium ion conductivity and structural stability of yttrium-substituted $\text{Li}_7\text{La}_3\text{Zr}_2\text{O}_{12}$. *Ionics* **2016**, *22*, 1281-1289.
25. Mukhopadhyay, S.; Thompson, T.; Sakamoto, J.; Huq, A.; Wolfenstine, J.; Allen, J. L.; Bernstein, N.; Stewart, D. A.; Johannes, M. Structure and stoichiometry in supervalent doped $\text{Li}_7\text{La}_3\text{Zr}_2\text{O}_{12}$. *Chemistry of Materials* **2015**, *27*, 3658-3665.
26. David, I. N.; Thompson, T.; Wolfenstine, J.; Allen, J. L.; Sakamoto, J. Microstructure and Li-Ion Conductivity of Hot-Pressed Cubic $\text{Li}_7\text{La}_3\text{Zr}_2\text{O}_{12}$. *Journal of the American Ceramic Society* **2015**, *98*, 1209-1214.
27. Baek, S. W.; Lee, J. M.; Kim, T. Y.; Song, M. S.; Park, Y. Garnet related lithium ion conductor processed by spark plasma sintering for all solid state batteries. *Journal of Power Sources* **2014**, *249*, 197-206.
28. Amores, M.; Ashton, T. E.; Baker, P. J.; Cussen, E. J.; Corr, S. A. Fast microwave-assisted synthesis of Li-stuffed garnets and insights into Li diffusion from muon spin spectroscopy. *Journal of Materials Chemistry A* **2016**, *4*, 1729-1736.
29. Murugan, R.; Ramakumar, S.; Janani, N. High conductive yttrium doped $\text{Li}_7\text{La}_3\text{Zr}_2\text{O}_{12}$ cubic lithium garnet. *Electrochemistry Communications* **2011**, *13*, 1373-1375.
30. Kumazaki, S.; Iriyama, Y.; Kim, K.-H.; Murugan, R.; Tanabe, K.; Yamamoto, K.; Hirayama, T.; Ogumi, Z. High lithium ion conductive $\text{Li}_7\text{La}_3\text{Zr}_2\text{O}_{12}$ by inclusion of both Al and Si. *Electrochemistry Communications* **2011**, *13*, 509-512.
31. Li, Y.; Cao, Y.; Guo, X. Influence of lithium oxide additives on densification and ionic conductivity of garnet-type $\text{Li}_6\text{.75La}_3\text{Zr}_1\text{.75Ta}_0\text{.25O}_{12}$ solid electrolytes. *Solid State Ionics* **2013**, *253*, 76-80.
32. Tadanaga, K.; Takano, R.; Ichinose, T.; Mori, S.; Hayashi, A.; Tatsumisago, M. Low temperature synthesis of highly ion conductive $\text{Li}_7\text{La}_3\text{Zr}_2\text{O}_{12}$ - Li_3BO_3 composites. *Electrochemistry Communications* **2013**, *33*, 51-54.
33. Janani, N.; Ramakumar, S.; Kannan, S.; Murugan, R. Optimization of lithium content and sintering aid for maximized Li^+ conductivity and density in Ta-doped $\text{Li}_7\text{La}_3\text{Zr}_2\text{O}_{12}$. *Journal of the American Ceramic Society* **2015**, *98*, 2039-2046.

34. Jonson, R. A.; McGinn, P. J. Tape casting and sintering of $\text{Li}_7\text{La}_3\text{Zr}_1.75\text{Nb}_0.25\text{Al}_0.1\text{O}_{12}$ with Li_3BO_3 additions. *Solid State Ionics* **2018**, *323*, 49-55.
35. Rosero-Navarro, N. C.; Yamashita, T.; Miura, A.; Higuchi, M.; Tadanaga, K. Effect of sintering additives on relative density and Li-ion conductivity of Nb-doped $\text{Li}_7\text{La}_3\text{ZrO}_{12}$ solid electrolyte. *Journal of the American Ceramic Society* **2017**, *100*, 276-285.
36. Hu, Z.; Liu, H.; Ruan, H.; Hu, R.; Su, Y.; Zhang, L. High Li-ion conductivity of Al-doped $\text{Li}_7\text{La}_3\text{Zr}_2\text{O}_{12}$ synthesized by solid-state reaction. *Ceramics International* **2016**, *42*, 12156-12160.